

High Precision Electron and Muon Reconstruction Performance with ATLAS at LHC Run-2

Fudong He^{a,*} for the ATLAS collaboration

*^aUniversity of Science and Technology of China,
No.96, JinZhai Road Baohe District, Hefei, Anhui, P.R. China.*

E-mail: fudong.he@cern.ch

Lepton reconstruction performance plays a crucial role in the measurement precision and new-physics search sensitivity of the Large Hadron Collider (LHC) data analysis of the ATLAS experiment. The 139 fb^{-1} of proton-proton collision data collected during the LHC Run-2 introduce both a challenge and an opportunity for detector performance studies. Using di-electron and di-muon resonances we are able to calibrate to sub per-mil accuracy the detector response for electrons and muons. This talk will present recently released results significantly improving the measurement of lepton reconstruction, identification and calibration performance with innovative techniques. New analysis techniques are exploited which involve multivariate analyses for rejecting background hadrons that mimic prompt leptons from the hard interactions as well as innovative in-situ corrections on data that reduce biases induced by residual detector displacements in muon momenta measurements. These improvements can further help extend the reach of ATLAS physics program.

*41st International Conference on High Energy physics - ICHEP2022
6-13 July, 2022
Bologna, Italy*

*Speaker

1. Introduction

During the years from 2015 to 2018, Run 2 of the Large Hadron Collider (LHC) at CERN provided an unprecedented number of pp collision events at a centre-of-mass energy of 13 TeV. The ATLAS detector [1] at the LHC is a multi-purpose particle detector covering nearly the entire solid angle around the collision point. The identification and accurate measurement of electrons and muons play a fundamental role in searches for new particles, in the measurement of Standard Model cross-sections, and in the precise measurement of the properties of fundamental particles such as the Higgs and W bosons and the top quark.

Compared to previous ATLAS papers [2] [3], the electron and muon reconstruction and identification techniques have been developed and improved accordingly for the dataset collected during Run 2. The results have been published in Ref. [4] and [5]. The most important modification for the electron reconstruction is the transition from fixed-size clusters of calorimeter cells towards a dynamical, topological cell clustering algorithm. The algorithms used for the identification of the electron candidates and the estimation of their energy have been updated accordingly. The muon identification algorithms and efficiency measurement have been improved dedicatedly for extreme regions of the phase space, such as p_T of a few GeV or a few TeV, the forward region of the detector where instrumentation coverage is poorer, or an environment polluted by a large number of pp interactions.

2. Electron reconstruction

An electron is defined as an object consisting of a cluster built from energy deposits in the calorimeter and a matched track (or tracks). Track reconstruction for electrons is unchanged with respect to Ref. [2]. In replacement of the sliding-window algorithm previously exploited in ATLAS for the reconstruction of fixed-size clusters of calorimeter cells the offline electron and photon reconstruction has been improved to use dynamic, variable-size clusters, called superclusters. Dynamic clusters change in size as needed to recover energy from bremsstrahlung photons or from electrons from photon conversions, and therefore lead to improved precision of energy measurement.

The reconstruction of electrons is started by the algorithm that prepares the tracks and clusters it will use. It selects clusters of energy deposits measured in topologically connected electromagnetic (EM) and hadronic calorimeter cells [6], denoted topo-clusters. These clusters are matched to ID tracks, which are re-fitted accounting for bremsstrahlung. A track is considered matched if, with either momentum magnitude, $|\eta_{\text{cluster}} - \eta_{\text{track}}| < 0.05$ and $-0.10 < q \times (\phi_{\text{track}} - \phi_{\text{cluster}}) < 0.05$, where q refers to the reconstructed charge of the track. The requirement on $q \times (\phi_{\text{track}} - \phi_{\text{cluster}})$ is asymmetric because tracks sometimes miss some energy from radiated photons that clusters measure. The supercluster-building steps are then performed, as described in Section 2.1, using the matched clusters as input for the electron candidates. After applying initial position corrections and energy calibrations to the resulting superclusters, the supercluster-building algorithm matches tracks to the electron superclusters. The electron objects to be used for analyses are then built.

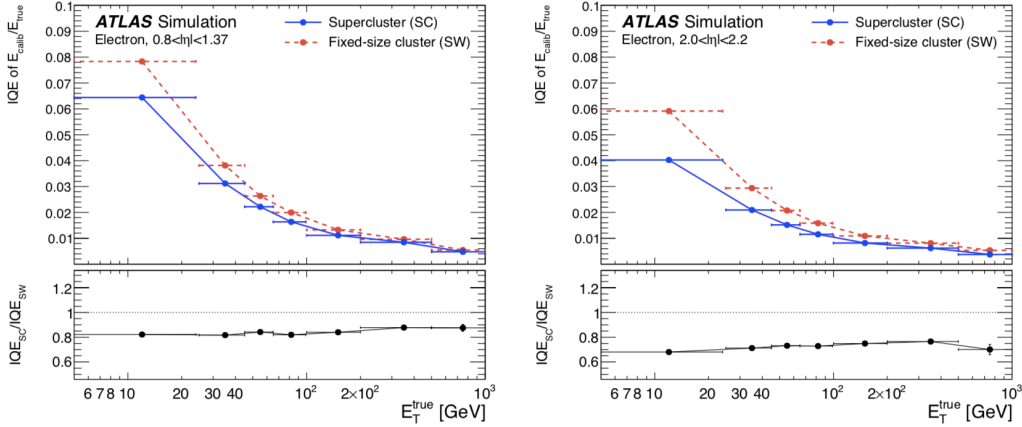


Figure 1: Calibrated energy response resolution, expressed in terms of IQE that is defined in Eq. 1 for electrons simulated with $\langle \mu \rangle = 0$. Two representative pseudorapidity ranges are shown [4].

2.1 Supercluster reconstruction

The electron supercluster reconstruction proceeds in two stages: in the first stage, EM topo-clusters are tested for use as seed cluster candidates, which form the basis of superclusters. For a cluster to become an electron supercluster seed, it is required to have a minimum E_T of 1 GeV and must be matched to a track with at least four hits in the silicon tracking detectors. In the second stage, EM topo-clusters near the seed candidates are identified as satellite cluster candidates, which may emerge from bremsstrahlung radiation or topo-cluster splitting. Satellite clusters are added to the seed candidates to form the final superclusters if they satisfy the necessary selection criteria. The seed clusters with their associated satellite clusters are called superclusters.

After the supercluster is reconstructed, the initial energy calibration is applied to the electron candidate to recover energy loss out of the cluster and passive material. The superclusters collect more deposited energy and improve the electron energy resolution, as shown in Figure 1. The IQE is used to quantify the width (resolution) of the energy response, defined as

$$\text{IQE} = \frac{Q_3 - Q_1}{1.349} \quad (1)$$

where Q_1 and Q_3 are the first and third quartiles of the distribution of $E_{\text{calib}}/E_{\text{true}}$, and the normalization factor is chosen such that the IQE of a Gaussian distribution would equal its standard deviation.

3. Electron calibration

The energy calibration of electrons closely follows the procedure used in Ref. [6], updated for the new electron energy reconstruction. The energy resolution of the electron is optimized using a multivariate regression algorithm based on the properties of the shower development in the EM calorimeter [4]. The energy scale correction, α , and energy resolution correction, c , are

parameterised as function of η . They are applied to the data and simulation as follows:

$$E^{\text{data, corr}} = E^{\text{data}}(1 + \alpha_i), \quad \left(\frac{\sigma_E}{E}\right)^{\text{MC, corr}} = \left(\frac{\sigma_E}{E}\right)^{\text{MC}} \oplus c_i \quad (2)$$

where i denotes different η bins, and the symbol \oplus denotes a sum in quadrature.

4. Electron identification

The identification of prompt electrons relies on a likelihood discriminant constructed from quantities measured in the inner detector, the calorimeter and the combined inner detector and calorimeter. A detailed description is given in Ref. [7]. A given set of requirements for the leptons is referred to as a selection working point (WP). Three electron identification WPs *Loose*, *Medium* and *Tight* are provided to suit a wide range of analyses and topologies. Figure 2 shows the resulting efficiencies in 2015-2018 Run 2 LHC data.

5. Muon reconstruction

The main signature exploited for muon reconstruction is that of a minimum-ionizing particle, as revealed by presence of a track in the Muon Spectrometer (MS) or characteristic energy deposits in the calorimeters. Global muon reconstruction is based primarily on information from the Inner Detector (ID) and MS tracking detectors as well as the calorimeters. There are five main muon reconstruction strategies, leading to the corresponding muon types: combined (CB), inside-out combined (IO), muon-spectrometer extrapolated (ME), segment-tagged (ST), and calorimeter-tagged (CT) [5]. The CB muon is the most common strategies. It will re-fit both ID and MS tracks to one single track. The other strategies aim to recover the efficiency for some special purposes.

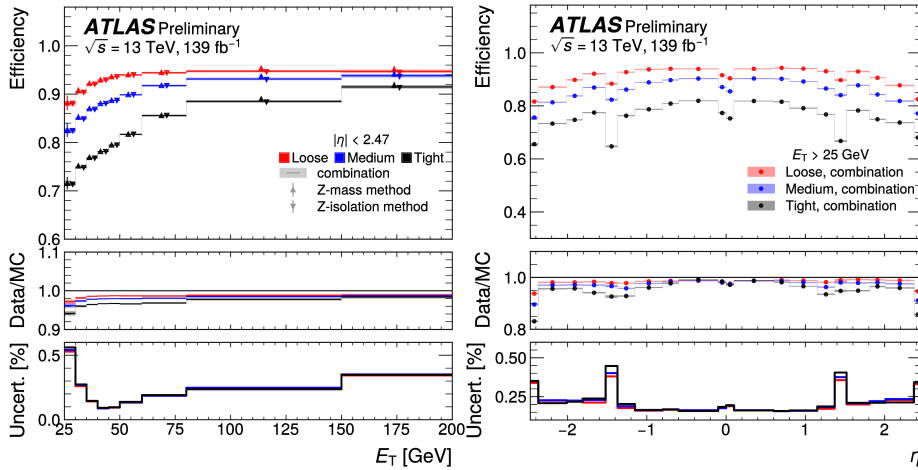


Figure 2: Efficiencies of the different identification working points for electrons in 2015-2018 Run 2 LHC data $Z \rightarrow ee$ events as a function of the electron transverse energy E_T (left) and as a function of the electron pseudorapidity η (right) [8].

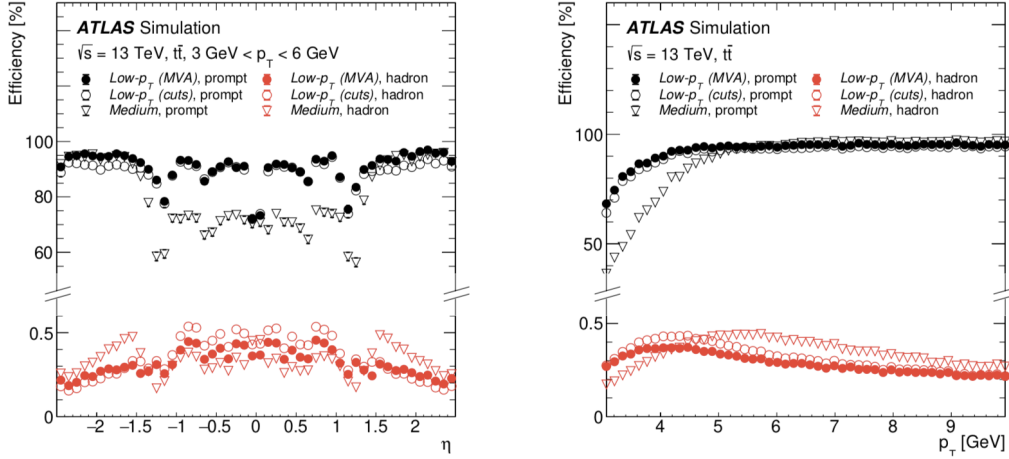


Figure 3: Muon identification efficiency as a function of η (left) and p_T (right) of the ID track for the *Low* – p_T and *Medium* WP requirements in simulated $t\bar{t}$ events, shown separately for prompt muons and muons from light hadron decays. The efficiency is calculated as the fraction of ID tracks that are associated with a reconstructed muon passing the given WP requirements. The ID tracks are matched, respectively, to generator-level prompt muons or light hadrons [5].

6. Muon identification

After reconstruction, high-quality muon candidates used for physics analyses are selected by a set of requirements on the number of hits in the different ID subdetectors and different MS stations, on the track fit properties, and on variables that test the compatibility of the individual measurements in the two detector systems. Three standard selection WPs are designed to cover the needs of the majority of physics analyses. The *Loose* selection WP was optimised for maximal efficiency. The *Medium* WP provides an efficiency and purity suitable for a wide range of analyses, while keeping the systematic uncertainties in the prompt-muon efficiency and background rejection small. Finally, the *Tight* selection WP provides largest power of hadron rejection.

Two additional selection WPs are designed for analyses targeting extreme phase space regions. The *High* – p_T WP ensures an optimal momentum measurement for muons with p_T above 100 GeV. The *Low* – p_T targets the lowest- p_T muons. Two versions of the *Low* – p_T WP have been developed: a *cut-based* selection, which reduces the kinematic dependencies of the background efficiencies, simplifying the implementation of data-driven estimates, and a *multivariate* (MVA) WP, maximising the overall performance. The performance of the cut-based and multivariate *Low* – p_T selection WPs in simulation is compared with that of the *Medium* selection WP in Figure 3.

7. Muon efficiency measurements

Two different methods are used to measure the muon reconstruction, identification, isolation and vertex association efficiencies with high precision in the $|\eta| < 2.5$ and $2.5 < |\eta| < 2.7$ regions respectively.

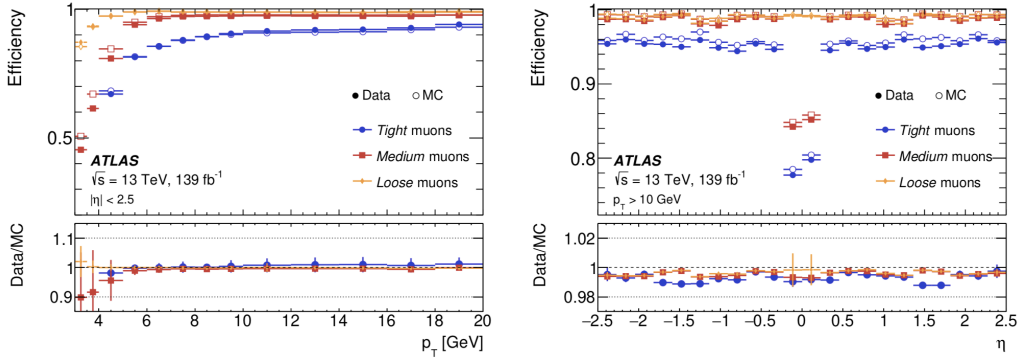


Figure 4: Muon reconstruction and identification efficiencies for the *Loose*, *Medium* and *Tight* criteria. The left plot shows the efficiencies measured in $J/\psi \rightarrow \mu\mu$ events as function of p_T . The right plot displays the efficiencies measured in $Z \rightarrow \mu\mu$ events as a function of η , for muons with $p_T > 10$ GeV [5].

In the $|\eta| < 2.5$ region, the tag-and-probe method is used and performed with a sample containing dimuon pairs. The tag muon is required to satisfy stringent identification criteria and to have triggered the online event selection. The second muon candidate in the pair, the probe, is used to test the efficiency of a certain reconstruction algorithm or of certain selection criteria. The muon reconstruction and identification efficiencies are measured with $Z \rightarrow \mu\mu$ events (mainly for $p_T > 10$ GeV) and $J/\psi \rightarrow \mu\mu$ events (mainly for p_T within 3–20 GeV). Figure 4 shows the muon reconstruction and identification efficiency for *Loose*, *Medium*, and *Tight* muons.

As the ID coverage is limited to $|\eta| < 2.5$, a tag-and-probe method involving the two independent detectors is not a viable option in $2.5 < |\eta| < 2.7$ region. The double-ratio method as described in Ref. [9] is used.

8. Conclusion

The reconstruction of electrons based on a dynamical, topological cell clustering algorithm has been described, and the corresponding updates to the methods used for the estimation of their energy have been discussed. Supercluster method is introduced in the electron reconstruction and improves the energy resolution by up to 30%. The identification of electrons has been revisited to match the improved cell clustering procedure.

The muon reconstruction and identification have been re-optimized for data recorded by the ATLAS detector between 2015 and 2018. The multivariate *Low*– p_T identification WP for extremely low p_T muons has been described. Compared to the *Medium* selection muon WP, the multivariate *Low*– p_T WP accepts an additional 18% of the prompt muons with $3 \text{ GeV} < p_T < 5 \text{ GeV}$, while the corresponding increase of the number of light hadrons is approximately 0.1%.

The corresponding electron and muon identification efficiencies have been measured using 139 fb^{-1} of pp collision data at $\sqrt{s} = 13 \text{ TeV}$ recorded between 2015 and 2018 by the ATLAS detector.

The present results define the baseline performance of the ATLAS detector for searches and measurements using electrons and muons from LHC proton–proton collision data collected at $\sqrt{s} = 13 \text{ TeV}$.

References

- [1] ATLAS Collaboration, *The ATLAS Experiment at the CERN Large Hadron Collider*, *JINST* **3** (2008) S08003.
- [2] ATLAS Collaboration, *Electron and photon energy calibration with the ATLAS detector using 2015–2016 LHC proton–proton collision data*, *JINST* **14** (2019) P03017 [arXiv:1812.03848].
- [3] ATLAS Collaboration, *Muon reconstruction performance of the ATLAS detector in proton–proton collision data at $\sqrt{s} = 13$ TeV*, *Eur. Phys. J. C* **76** (2016) 292 [arXiv:1603.05598].
- [4] ATLAS Collaboration, *Electron and photon performance measurements with the ATLAS detector using the 2015–2017 LHC proton–proton collision data*, *JINST* **14** (2019) P12006 [arXiv:1908.00005].
- [5] ATLAS Collaboration, *Muon reconstruction and identification efficiency in ATLAS using the full Run 2 pp collision data set at $\sqrt{s} = 13$ TeV*, *Eur. Phys. J. C* **81** (2021) 578 [arXiv:2012.00578].
- [6] ATLAS Collaboration, *Topological cell clustering in the ATLAS calorimeters and its performance in LHC Run 1*, *Eur. Phys. J. C* **77** (2017) 490 [arXiv:1603.02934].
- [7] ATLAS Collaboration, *Electron reconstruction and identification in the ATLAS experiment using the 2015 and 2016 LHC proton–proton collision data at $\sqrt{s} = 13$ TeV*, *Eur. Phys. J. C* **79** (2019) 639 [arXiv:1902.04655].
- [8] ATLAS Collaboration, *Electron efficiency with full Run2*, , <https://atlas.web.cern.ch/Atlas/GROUPS/PHYSICS/PLOTS/EGAM-2022-02>, 2022.
- [9] ATLAS Collaboration, *Measurement of the muon reconstruction performance of the ATLAS detector using 2011 and 2012 LHC proton–proton collision data*, *Eur. Phys. J. C* **74** (2014) 3130 [arXiv:1407.3935].